J. Fluid Mech. (1979), *vol.* 92, *part* 3, *pp.* 435–457
Printed in Great Britain

Enhanced sedimentation in settling tanks with inclined walls

By ANDREAS ACRIVOS
AND
ERIC HERBOLZHEIMER
Department of Chemical Engineering, Stanford University, California 94305

(Received 13 March 1978 and in revised form 27 November 1978)

Using the principles of continuum mechanics, a theory is developed for describing quantitatively the sedimentation of small particles in vessels having walls that are inclined to the vertical. The theory assumes that the flow is laminar and that the particle Reynolds number is small, but c_0, the concentration in the suspension, and the vessel geometry are left arbitrary. The settling rate S is shown to depend upon two dimensionless groups, in addition to the vessel geometry: a sedimentation Reynolds number R, typically $O(1)$–$O(10)$; and Λ, the ratio of a sedimentation Grashof number to R, which is typically very large. By means of an asymptotic analysis it is then concluded that, as $\Lambda \to \infty$ and for a given geometry, S can be predicted from the well-known Ponder–Nakamura–Kuroda formula which was obtained using only kinematic arguments. The present theory also gives an expression for the thickness of the clear-fluid slit that forms underneath the downward-facing segment of the vessel walls, as well as for the velocity profile both in this slit and in the adjoining suspension.

The sedimentation rate and thickness of the clear-fluid slit were also measured in a vessel consisting of two parallel plates under the following set of conditions: $c_0 \leqslant 0{\cdot}1$, $R \sim O(1)$, $O(10)^5 \leqslant \Lambda \leqslant O(10^7)$ and $0° \leqslant \alpha \leqslant 50°$, where α is the angle of inclination. Excellent agreement was obtained with the theoretical predictions. This suggests that the deviations from the Ponder–Nakamura–Kuroda formula reported in the literature are probably due to a flow instability which causes the particles to resuspend and thereby reduces the efficiency of the process.

1. Introduction

The removal of solid particles from liquid streams constitutes an important step in a large variety of industrial processes. The simplest and most common method of achieving this is by means of gravity settling which, however, often requires large tanks especially when the particles in the suspension are small. Thus, a need exists for designing settling devices which have retention times on the order of minutes rather than hours.

One potentially very promising class of devices is based on the application of the 'Boycott effect', a curious phenomenon of settling convection in inclined vessels first reported by Boycott (1920). The essence of Boycott's observation was that '... if oxalated or defibrinated blood is put to stand in narrow tubes, the corpuscles sediment a good deal faster if the tube is inclined than when it is vertical'. Subsequently, many investigators studied the phenomenon for a variety of suspensions and reported that

0022-1120/79/4238-6650 $02.00

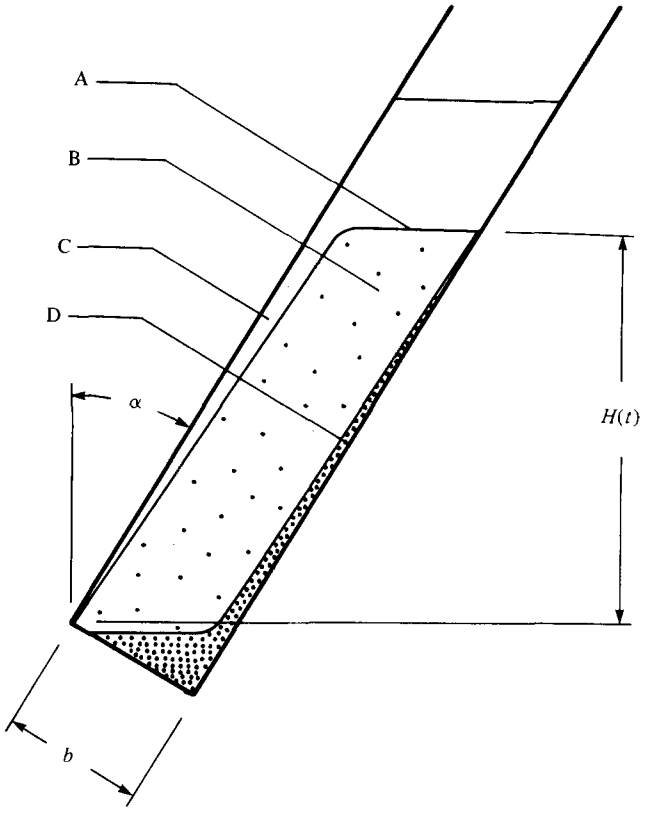

FIGURE 1. The different regions in the flow field: A, interface between the particle-free fluid and the suspension; B, suspension; C, particle-free fluid layer; D, concentrated sediment layer on upward-facing surface.

a several-fold increase in the sedimentation rate could thereby be achieved. An excellent summary of the earlier papers on the subject is given by Hill (1974).

A qualitative explanation of the 'Boycott effect' can be obtained by assuming that, even when the walls of the container are inclined, the particles merely settle vertically until they reach the upward-facing surface. Then, whereas in settling between vertical parallel plates a particle must travel a distance of $O(H)$ (cf. figure 1) to be removed, this distance is only $O(b)$ when the plates are inclined. Thus, assuming that the particles can flow down the upward-facing inclined plate and be collected at the bottom, one is led to the conclusion that the enhancement to the settling rate should be $O(H/b)$. Surprisingly, this prediction is correct under some circumstances even though, as we shall see below, the process of sedimentation in inclined vessels is significantly more complicated than simple vertical settling.

To begin we note that, if the particles just settled vertically, particle-free fluid would appear above the suspension both at the top of the vessel and directly under the downward-facing surface, and that every point on the interface separating the clear fluid region from the suspension would fall vertically with velocity v_0, the particle settling velocity of the same suspension as measured in a container with vertical walls. Experimental observations of the inclined settling process show, however, a markedly

different behaviour. First of all, although a clear-fluid layer does form under the downward-facing plate (cf. figure 1), its thickness remains small and is essentially independent of time. Also, although a sharp, effectively horizontal interface between the suspension and the clear fluid does exist on top (as in vertical settling), this interface falls with an enhanced vertical velocity that is typically several times greater than v_0.

A kinematic model based on these experimental observations which led to a quantitative prediction for the sedimentation rate was presented by Ponder (1925) and independently by Nakamura & Kuroda (1937) and will be referred to henceforth as the PNK theory. These authors argued that, since the thickness of the liquid layer under the downward-facing surface is typically observed to be small and independent of time, the portion of clarified fluid formed under this surface should be instantaneously added to the clear fluid above the horizontal interface. Thus, the vessel is assumed to remain filled with suspension everywhere below a horizontal interface which moves with an enhanced velocity (i.e. a velocity greater than v_0). The volumetric rate at which clarified fluid is formed then equals v_0 times the cross-sectional area of the vessel at the top of the suspension plus the horizontally projected area of the downward-facing surface below the top of the suspension. Of course, this volumetric settling rate must equal the area of the interface at the top of the suspension times its vertical velocity.

For inclined settling between parallel plates (i.e. in a container as shown in figure 1) these results become the more familiar expressions

$$S(t) = \frac{v_0 b}{\cos\alpha}\left(1+\frac{H}{b}\sin\alpha\right), \tag{1.1}$$

$$\frac{dH}{dt} = -v_0\left(1+\frac{H}{b}\sin\alpha\right), \tag{1.2}$$

where $S(t)$ is the volumetric rate at which clarified fluid is formed per unit depth in the third dimension of the vessel (hereafter referred to as the settling rate) and $H(t)$ is the instantaneous height of the suspension, α is the constant angle of inclination and b is the spacing between the plates as shown in figure 1. Thus, according to the PNK theory, the enhancement to the velocity of the interface is $(H/b)\sin\alpha$ which, of course, can in principle be made arbitrarily large by choosing the appropriate aspect ratio H/b for a given angle of inclination.

Several experimental studies have been performed to date on sedimentation in tilted tubes and beneath inclined boundaries (e.g. Kinosita 1949; Pearce 1962; Graham & Lama 1963; Oliver & Jenson 1964; Vohra & Ghosh 1971; Zahavi & Rubin 1975). For some systems, the results were found to be in good agreement with (1.1) and (1.2) while for others the agreement was poor. In general, there seems to be a consensus in the literature that the PNK theory gives an upper bound to the settling rate although both Zahavi & Rubin (1975) and Kinosita (1949) have reported higher rates under some conditions. Kinosita (1949), who undertook one of the more complete experimental projects on the subject, also noted the existence of strong convection currents forming a vortex in the suspended phase with particle velocities as high as 100 times the sedimentation velocity.

A few attempts have also been made to extend the PNK theory using more elaborate kinematic models (Graham & Lama 1963; Oliver & Jenson 1964; Vohra & Ghosh 1971; Zahavi & Rubin 1975), which led to equations somewhat more involved than (1.1) and (1.2). However since all these expressions contain adjustable parameters which in general are complicated functions of concentration and of the geometry of the vessel and must be evaluated by finding the best fit to inclined settling data, the usefulness and significance of these extensions of the PNK theory is unclear.

All such purely kinematic models suffer from at least two serious limitations. Clearly, they can provide no information about such flow characteristics as the state of motion and concentration distribution within the suspension, the thickness of the thin fluid layer beneath the downward-facing surface, etc. But more importantly, their range of validity is unknown. Thus, for example, equations (1.1) and (1.2) cannot be used for design purposes with any degree of confidence since it is impossible to tell *a priori*, on the basis of the PNK theory, under what set of conditions, if any, they can be expected to apply. Evidently then, a more fundamental approach is required.

An important contribution to the subject was the recent work of Hill (1974) and of Hill, Rothfus & Li (1977) who, to the authors' knowledge, were the first to study the phenomenon theoretically using the appropriate equations of continuum mechanics. Hill *et al.* limited their investigation to very dilute suspensions of solid spheres under conditions of negligibly small particle Reynolds numbers. Hence, the settling velocity of the individual particles is given by Stokes' law

$$u_0 = \tfrac{2}{9}a^2(\rho_s - \rho_f)g/\mu, \tag{1.3}$$

where a is the radius of the spheres, ρ_s is their density, ρ_f is the density of the fluid, μ is the viscosity of the fluid, and g is the gravitational constant. On using dimensional analysis, it is easy to show (cf. § 3 below) that, aside from the geometric factors such as the shape of the container and the angle of inclination, the process is governed by two dimensionless groups: R, a sedimentation Reynolds number, and Λ, the ratio of a sedimentation Grashof number to R,

$$\left.\begin{aligned} R &\equiv l\rho_f u_0/\mu = \tfrac{2}{9}l\,a^2\rho_f(\rho_s-\rho_f)g/\mu^2, \\ \Lambda &= l^2 g(\rho_s-\rho_f)c_0/u_0\mu = \tfrac{9}{2}(l/a)^2 c_0, \end{aligned}\right\} \tag{1.4}$$

where l is a characteristic length of the macroscale motion (which Hill *et al.* (1977) took to be the initial height of the suspension), and c_0 is the initial volume fraction of solids which is assumed to be initially uniform. Hill *et al.* (1977) obtained numerical solutions to the appropriate equations of motion for this system and determined the sedimentation rates in various upward-pointing cones. They also performed experiments, the results of which compared favourably with their theoretical predictions. The range of parameters covered by Hill, Rothfus & Li's work are: (i) theory: $0{\cdot}8 < R < 6{\cdot}5$, $250 < \Lambda < 25000$, $30° < \alpha < 43°$; (ii) experiments: $0{\cdot}8 < R < 1{\cdot}5$, $2800 < \Lambda < 29000$, $30° < \alpha < 43°$, and $2\times10^{-7} < c_0 < 2\times10^{-3}$. These authors confirmed the existence of a rapid convective motion within the main body of the suspension [already noted by Kinosita (1949)] and measured the corresponding particle velocities, which they found to be $O(10\,u_0)$. Finally, by extrapolating their results, these authors concluded that the PNK theory gave the correct expression for the settling

rate in the dual limit $\Lambda \to \infty$ and $R \to 0$, but of course such a conclusion can only be viewed as tentative on account of the limited range and accuracy of the numerical solutions and experiments in their work.

In the present paper, we shall investigate this phenomenon theoretically using analytical techniques. Our treatment will be limited to suspensions of identical spheres, laminar flow, and negligibly small particle Reynolds numbers (the same conditions as in Hill, Rothfus & Li's study) but the geometry of the settling vessel as well as the concentration will be left arbitrary. Although for simplicity most of the analysis will be developed for two-dimensional vessels only, the extension to three-dimensional flows is straightforward and the principal conclusions to be obtained below carry over to the three-dimensional case with little or no change.

We shall consider in detail the case $\Lambda \gg 1$ with $R\Lambda^{-\frac{1}{3}} < O(1)$ and shall show that, as $\Lambda \to \infty$ and provided the flow remains laminar, the settling rate is that given by the PNK theory. Furthermore, we shall derive expressions for the velocity fields both within the clear-fluid slit underneath the downward-facing surface as well as in the bulk of the suspension. Our results then will yield a fairly complete quantitative picture of the settling operation under these circumstances, but more importantly, they will provide a sound basis for extending the analysis to a more general set of conditions where the simplifying assumptions of the present work no longer hold. We shall also discuss briefly the application of our theory to the industrially important process of continuous inclined settling. Finally, the results of our analysis will be compared with observations of inclined settling experiments which were performed in our laboratory.

2. Kinematics

We begin by showing that several important results can be derived which are independent of the details of the flow field. We treat the suspension as an effective fluid and express the ensemble-averaged fluid and particle velocities in terms of the bulk average velocity, $\mathbf{u}$, and the average slip velocity, $\mathbf{u}_s$, defined as

$$\mathbf{u} = (1-c)\,\mathbf{u}_f + c\mathbf{u}_p, \tag{2.1a}$$

$$\mathbf{u}_s = \mathbf{u}_p - \mathbf{u}, \tag{2.1b}$$

where c is the local volume fraction of solids.

Assuming that the particles and fluid are incompressible, the dimensionless ensemble-averaged fluid and particle continuity equations can be combined to give

$$\nabla . \mathbf{u} = 0 \tag{2.2}$$

and

$$\partial\phi/\partial t + \mathbf{u}_p . \nabla\phi = -\phi \nabla . \mathbf{u}_s, \tag{2.3}$$

where ϕ is the local volume fraction of solids divided by c_0, a characteristic value of the volume fraction in the suspension, typically the initial value. In the above, and in what follows, all velocities have been made dimensionless by division by v_0, the average settling velocity in a container with vertical walls of an individual sphere in the suspension with volume fraction c_0, all position co-ordinates by division by some as yet unspecified length scale l (typically a characteristic height of the suspension), and the time by division by l/v_0.

We shall now restrict our attention to flows in which the Reynolds number based on the relative motion between the particles and the fluid is negligibly small: a condition that is satisfied in most systems of practical interest owing to the small size and settling velocity of the suspended particles. With this restriction, the interaction between the particles and the fluid appears only in the drag which must be balanced by the gravitational force on the particles due to their excess weight. Hence, if we suppose that the effects of particle–particle interactions depend only on the local particle concentration, we can define a function $f(c)$ such that the dimensional slip velocity $\mathbf{u}_s^*$ is given by

$$\mathbf{u}_s^* = u_0 f(c)\,\mathbf{e}, \tag{2.4}$$

where u_0 is the Stokes velocity as given by (1.3), $\mathbf{e}$ is the unit vector in the direction of gravity, and $f(c)$ is a monotonically decreasing function with $f(0) = 1$. Then, by definition, $v_0 = u_0 f(c_0)$ so the dimensionless slip velocity is

$$\mathbf{u}_s = F(c)\,\mathbf{e}, \tag{2.5}$$

where

$$F(c) = f(c)/f(c_0).$$

Substituting (2.5) into the particle continuity equation (2.3) yields

$$\partial\phi/\partial t + \mathbf{u}_p \cdot \nabla\phi = -c_0\,\phi F'(c)\,\mathbf{e}\cdot\nabla\phi \tag{2.6}$$

where

$$F'(c) = dF/dc \sim O(1).$$

Let us next consider the case when ϕ is initially equal to unity everywhere within the suspension, which is the usual initial condition for batch sedimentation.† Then initially, the right-hand side of (2.6) vanishes identically everywhere except on a surface where ϕ undergoes a jump from 0 to 1 (at $t = 0$ this surface usually coincides with the downward-facing wall and the top of the suspension) and near the upward-facing walls where ϕ rises to its maximum value ϕ_m. Hence, in view of (2.6), ϕ must be a constant along particle streamlines and, therefore, throughout the duration of the settling process $\phi \equiv 1$ within that portion of the flow field containing particles. This is true everywhere except near the upward-facing surface where the particle streamlines terminate and ϕ rises from 1 to ϕ_m. Although, as is well known from the theory of vertical sedimentation (Kynch 1952), this jump in concentration can broaden and cause concentration gradients to back up along the particle streamlines, it will be shown in the next section that when $\Lambda \gg 1$ the region within which ϕ increases above 1 is restricted to the bottom of the vessel and to a thin layer along the upward-facing surface. Consequently, when $\Lambda \gg 1$, we can subdivide the domain into three regions: (*a*) a particle-free region where $\phi \equiv 0$; (*b*) the core of the suspension where $\phi \equiv 1$; and (*c*) a region at the bottom of the vessel and a thin layer along the upward-facing surface where ϕ rises to its maximum value. We also note that the boundary between regions (*a*) and (*b*) is sharp, whereas the concentration may vary continuously in the sediment layer.

† Requiring the suspension to be initially uniform may appear to impose a severe limitation in this analysis. However, at the start of both vertical and inclined settling experiments, rapid small-scale mixing motions are invariably observed which seem to quickly smooth out any perturbations in the initial concentration distribution. Thus, it would appear that the settling operation proceeds as if the initial concentration in the suspension were uniform.

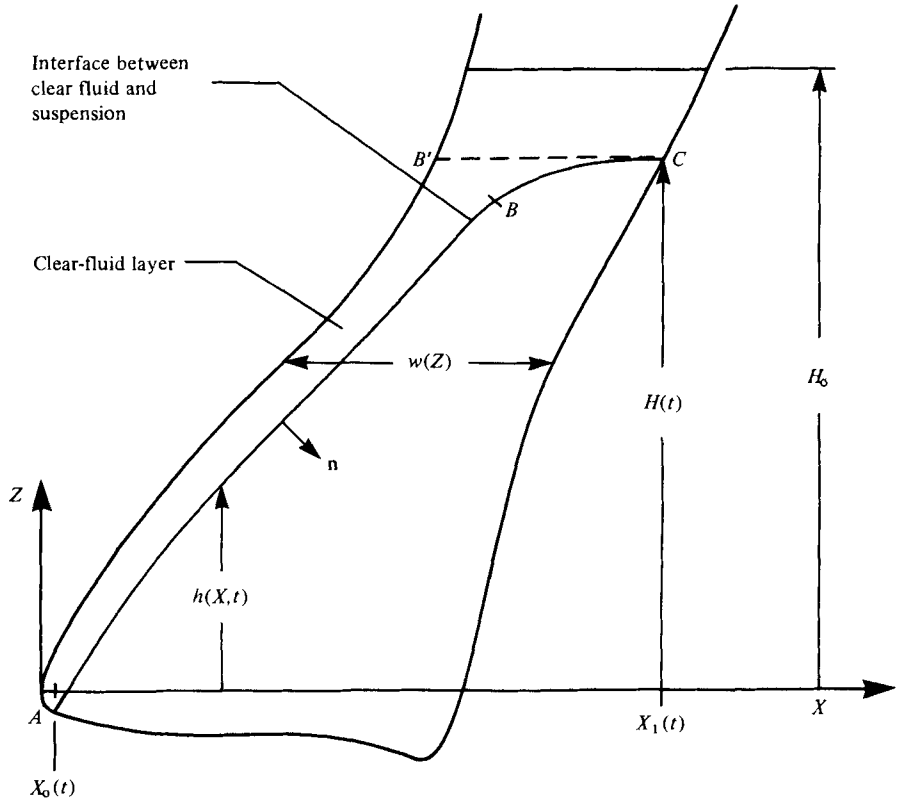

FIGURE 2. Definition of the variables used in the kinematic analysis.

The results derived so far have a number of interesting implications and lead directly to the PNK theory if certain well-defined conditions are met. For simplicity, we shall consider a two-dimensional vessel with one downward-facing and one upward-facing surface and shall define a Cartesian co-ordinate system X, Z with origin at the point of intersection between the two surfaces (cf. figure 2). The extension of the present analysis to more general vessel geometries is straightforward.

To begin with, let $h(X,t)-Z=0$ be the equation of the interface between the suspension and the particle-free fluid. Since the motion of this interface is determined by that of the particles, we find from the kinematic condition that, at $h = Z$,

$$(1+h_x^2)^{-\frac{1}{2}}\,\partial h/\partial t = -\mathbf{u}_p\,.\,\mathbf{n} = -(\mathbf{u}+\mathbf{u}_s)\,.\,\mathbf{n}, \tag{2.7}$$

using (2.1*b*) and with $\mathbf{n}$ being the inner unit normal. Integrating (2.7) along the interface ABC (cf. figure 2) and noting that ds, the corresponding line element, equals $(1+h_x^2)^{\frac{1}{2}}\,dX$, we obtain

$$-\int_{X_0}^{X_1}\frac{\partial h}{\partial t}\,dX = \int_A^C (\mathbf{u}\,.\,\mathbf{n})\,ds + \int_A^C \mathbf{u}_s\,.\,\mathbf{n}\,ds, \tag{2.8}$$

where A, C, $X_0(t)$, and $X_1(t)$ are as shown in figure 2. By use of the divergence theorem and the fact that $\mathbf{u}\,.\,\mathbf{n} = 0$ on the walls of the vessel, the second term of (2.8) equals the integral of $\nabla\,.\,\mathbf{u}$ over the volume of the region containing particles which, in view of

(2.2) vanishes identically. In addition, the left-hand side of (2.8) equals the dimensionless settling rate, $S(t)$, as defined in the last section. Thus, we obtain the general result

$$S(t) = \int_A^B \mathbf{u}_s . \mathbf{n}\, ds. \tag{2.9}$$

When the Reynolds number based on the relative motion of the particles and fluid is small, $\mathbf{u}_s$ is given by (2.5) and the settling rate is determined by the concentration on the interface. But since, as remarked earlier, $\phi \equiv 1$ everywhere in the suspension provided that $\Lambda \gg 1$, $\mathbf{u}_s = \mathbf{e}$ on the interface. Therefore, with $\mathbf{e}.\mathbf{n}\, ds = dX$ along AC, (2.9) becomes

$$S(t) = X_1(t) - X_0(t), \tag{2.10}$$

which is the same as the PNK result except for the $-X_0(t)$ term. We shall show in the next section, however, that $X_0(t)$ is at most $O(\Lambda^{-\frac{1}{2}})$ when Λ is large, and hence we can conclude that the settling rate as given by the PNK theory is correct, provided that (i) the suspension is monodisperse, (ii) the particle Reynolds number is small, (iii) the initial concentration distribution is uniform, (iv) Λ is large, and (v) the interface between the clear fluid layer and suspension remains stable.

Thus, contrary to the suppositions of previous workers, the PNK theory correctly predicts the instantaneous volumetric settling rate regardless of the details of the fluid motion (provided, of course, that the above conditions are satisfied); however, this conclusion does not imply that the PNK theory correctly predicts the movement of the interface whose position depends on the particle velocity. The latter must be found by solving the appropriate momentum equations. In § 3 we shall show that, when $\Lambda \gg 1$, (i) the particle-free layer underneath the downward-facing surface is infinitesimally thin; (ii) the interface between this thin layer and the suspension is stationary; and (iii) the remaining segment of the interface is horizontal. In other words, we shall show that the curve ABC of figure 2 can be approximated by $AB'C$ of which AB' is stationary and $B'C$ is horizontal with height $H(t)$. Thus when $\Lambda \gg 1$ all of the new particle-free fluid formed must accumulate at the top of the vessel and hence the PNK theory also predicts the interface motion correctly.

We close this section by showing briefly how the present analysis carries over to the case of continuous settling in which suspension of uniform concentration c_0 is introduced at a constant rate into the settling vessel while concentrated sediment and pure fluid are withdrawn from the bottom and top respectively. The precise location of the feed point is unimportant to a first approximation but, clearly, under efficient operating conditions, it will lie within the core of the suspension, i.e. somewhere below the curve ABC of figure 2, while the overflow of the particle-free fluid will be drawn off slightly above C. The present theory applies unchanged to this system except that h is now time independent so the left-hand side of (2.8) vanishes. Also, the second term of (2.8) is no longer zero but equals instead the difference between the volumetric rate at which concentrated suspension is removed from the bottom of the vessel and that at which suspension is fed into the system. But on account of the overall mass balance, this difference in flow rates must equal the rate at which particle-free fluid is produced and drawn off the top, i.e. S. Thus, in the general case, (2.9) is recovered once again and this reduces to (2.10) under the same conditions as before. Of course, in contrast to the case of batch settling, S and $X_1 - X_0$ are time independent and hence no further information is needed at this stage because, for a given vessel

shape, (2.10) gives the minimum size of equipment required to give a desired settling rate, or conversely, the maximum settling rate obtainable in a given vessel.

3. The details of the flow field

To obtain the equations of motion we take the ensemble average of the momentum equation and neglect the Reynolds stress terms relative to the bulk stress because the Reynolds number based on the flow around the particles is assumed to be small. We further assume that the suspension behaves like a Newtonian fluid with an effective viscosity depending only on the local volume fraction of particles. Under these conditions the ensemble-averaged momentum equations for a uniform particle concentration become

$$R\rho(\phi)\, D\mathbf{u}/Dt = -\nabla P - \Lambda(1-\phi)\,\mathbf{e} + \mu(\phi)\,\nabla^2\mathbf{u}, \tag{3.1}$$

where $\rho(\phi) \equiv 1 + c_0\phi(\rho_s/\rho_f - 1)$, $\mu(\phi)$ is the effective viscosity of the suspension divided by that of the pure fluid, and R and Λ are defined as in (1.4) except that $v_0 = u_0 f(c_0)$ replaces u_0. Finally, P is the dimensionless pressure corresponding to p (made dimensionless with $l/\mu v_0$) minus the dimensionless hydrostatic pressure head due to the suspension of concentration c_0, i.e.

$$\nabla P = \nabla p - \frac{gl^2}{\mu v_0}\,(c_0\rho_s + (1-c_0)\,\rho_f)\,\mathbf{e} = \nabla p - \Lambda\left(1 + \frac{1}{c_0}\,\frac{\rho_f}{\rho_s - \rho_f}\right)\mathbf{e}. \tag{3.1a}$$

Because of this definition for P, the body force on the suspension appears as a buoyancy term $-\Lambda(1-\phi)\,\mathbf{e}$, which tends to induce an upward motion in the suspension wherever the concentration is less than c_0 (i.e. $\phi < 1$) or conversely a downward flow wherever $\phi > 1$.

In the vast majority of cases, Λ is $O(10^5)$ or larger, if l is set equal to the instantaneous height of the suspension, and hence it appears advisable to consider the asymptotic solution of (3.1) as $\Lambda \to \infty$. Under these conditions, the buoyancy term in (3.1) clearly plays an important role. This term vanishes within the suspension, where $\phi \equiv 1$, but is large within the clear-fluid layer underneath the downward-facing surface where it induces strong velocity currents. In fact, the flow within this region is qualitatively similar to natural convection past a heated surface which, as is well known, is also induced by buoyancy forces.

3.1. *The particle-free layer*

We anticipate that the thickness of the particle-free layer becomes vanishingly small as $\Lambda \to \infty$ and hence we find it convenient to introduce the boundary-layer co-ordinates (x, y) with x denoting the co-ordinate along the downward-facing surface and y the co-ordinate normal to it. The corresponding velocity components are u and v.

Now, according to the kinematic condition (2.7), v is $O(1)$ along the interface between the suspension and the particle-free fluid, and hence it is similarly $O(1)$ within the clear-fluid layer. In turn, this implies from continuity that the longitudinal velocity u is, in order of magnitude, inversely proportional to the thickness of this layer. But since, on account of (3.1), the viscous forces must balance the buoyancy term in this region, it follows that $u = O(\Lambda^{\frac{1}{3}})$ and that the thickness of the layer is $O(\Lambda^{-\frac{1}{3}})$. We therefore define the following stretched variables,

$$\tilde{u} = \Lambda^{-\frac{1}{3}}u, \quad \tilde{v} = v, \quad \tilde{y} = \Lambda^{\frac{1}{3}}y, \quad \tilde{y} - \tilde{\delta}(x,t) = 0, \tag{3.2}$$

where the last expression represents the equation of the suspension/clear layer interface in the new scaled variables. Thus, we obtain in lieu of (3.1),

$$\frac{\partial^2\tilde{u}}{\partial\tilde{y}^2}+\cos\alpha(x)-\frac{1}{\Lambda}\frac{\partial P}{\partial x}=R\Lambda^{-\frac{1}{3}}\left\{\tilde{u}\frac{\partial\tilde{u}}{\partial x}+\tilde{v}\frac{\partial\tilde{u}}{\partial\tilde{y}}\right\}+O(R\Lambda^{-\frac{2}{3}})+O(\Lambda^{-\frac{1}{3}}) \tag{3.3a}$$

and

$$\Lambda^{-\frac{2}{3}}\,\partial P/\partial\tilde{y}+\sin\alpha(x)=O(\Lambda^{-\frac{1}{3}})+O(R\Lambda^{-\frac{2}{3}}), \tag{3.3b}$$

where $\alpha(x)$ is the local angle of inclination of the surface, which need not be planar. In addition we have for the continuity equation

$$\partial\tilde{u}/\partial x+\partial\tilde{v}/\partial\tilde{y}=0. \tag{3.3c}$$

In obtaining (3.3a)–(3.3c) all terms which arise in transforming to the boundary-layer co-ordinates due to the curvature of the surface have been assumed negligibly small which, for this analysis, requires that $d\alpha/dx=o(\Lambda^{\frac{1}{3}})$ everywhere. Thus, we shall consider only smooth surfaces which satisfy $d\alpha/dx=O(1)$, although this restriction is not essential to the development of our theory. Also, in most cases of practical interest, R is $O(1)$, i.e. $R\Lambda^{-\frac{1}{3}}=O(\Lambda^{-\frac{1}{3}})$ and hence, in what follows we shall neglect the first term on the right-hand side of (3.3a) although again this simplification is not essential to our analysis as will be shown at the close of § 3.2.

The boundary conditions are:

$$(a)\ \tilde{u}=\tilde{v}=0 \quad \text{at} \quad \tilde{y}=0, \tag{3.4a}$$

$$(b)\ \Lambda^{-\frac{1}{3}}\partial\tilde{\delta}/\partial t+\tilde{u}\,\partial\tilde{\delta}/\partial x-\tilde{v}=\sin\alpha(x) \quad \text{at} \quad \tilde{y}=\tilde{\delta}, \tag{3.4b}$$

$$(c)\ \partial\tilde{u}/\partial\tilde{y}=o(1) \quad \text{at} \quad \tilde{y}=\tilde{\delta}, \tag{3.4c}$$

where (3.4b) is the kinematic condition while justification for (3.4c) will be postponed until later in § 3.2.

By considering the motion in the suspension it will be shown in § 3.2 that P is at most $O(\Lambda^{\frac{2}{3}})$ at the interface $\tilde{y}=\tilde{\delta}$. Therefore, in view of (3.3b), the pressure within the clear-fluid layer is at most $O(\Lambda^{\frac{2}{3}})$ and the term $\Lambda^{-1}\partial P/\partial x$ in (3.3a) may be neglected at this stage of the analysis. Hence, the solution of (3.3) which satisfies (3.4a) and (3.4c) is

$$\tilde{u}=(\tilde{y}\tilde{\delta}-\tfrac{1}{2}\tilde{y}^2)\cos\alpha(x)+o(1), \tag{3.5a}$$

$$\tilde{v}=-\tfrac{1}{2}\tilde{y}^2\,d(\tilde{\delta}\cos\alpha)/dx+\tfrac{1}{6}\tilde{y}^3\,d(\cos\alpha)/dx+o(1). \tag{3.5b}$$

The equation for $\tilde{\delta}$

$$\Lambda^{-\frac{1}{3}}\partial\tilde{\delta}/\partial t+\tilde{\delta}^2\cos\alpha(x)\,\partial\tilde{\delta}/\partial x=\sin\alpha(x)+\tfrac{1}{3}\tilde{\delta}^3\sin\alpha(x)\,d\alpha/dx, \tag{3.6}$$

is then obtained by substituting (3.5a) and (3.5b) into the kinematic condition, (3.4b).

Equation (3.6) can be solved by the method of characteristics to determine the time dependent behaviour of the flow within the clear-fluid layer.† In order to simplify the analysis, we shall consider the special case when the downward-facing surface is flat (i.e. $\alpha(x)=\alpha$, a constant) although this method can also be used for general shapes. Introducing the characteristic curves along which

$$(\partial x/\partial\tau)_c=\tilde{\delta}^2\cot\alpha \tag{3.7}$$

† The use of pseudo-steady velocity profiles in (3.6) is justified by the fact that the time dependent terms in the momentum equation are $O(R\Lambda^{-\frac{2}{3}})$ and therefore negligible relative to the other terms in (3.6).

with $\tau \equiv t\Lambda^{\frac{1}{3}} \sin\alpha$, we obtain for (3.6) that

$$d\tilde{\delta}/d\tau = 1 \tag{3.8}$$

along a characteristic. Consider the initial and boundary conditions $\tilde{\delta}(x, 0) = 0$ and $\tilde{\delta}(0, \tau) = 0$. Then, along those characteristics which cross the x axis, (3.8) gives $\tilde{\delta}(x, \tau) = \tau$. On substituting this into (3.7) and integrating, we thus obtain for the shape of the characteristic with x intercept ξ

$$\tilde{\delta} = \tau = (3(x-\xi)\tan\alpha)^{\frac{1}{3}}. \tag{3.9}$$

Similarly, for the characteristic crossing the τ axis at τ_0 we find $\tilde{\delta}(x, \tau) = \tau - \tau_0$ and hence the shape of this characteristic is

$$\tilde{\delta} = \tau - \tau_0 = (3x\tan\alpha)^{\frac{1}{3}}. \tag{3.10}$$

It is apparent from (3.9) that, for fixed x, $\tilde{\delta}$ increases linearly with time until it reaches its steady-state value for that x (i.e. until the characteristic passing through the origin is reached) and that for larger times $\tilde{\delta}$ remains steady. Hence, at any given x, $\tilde{\delta}$ reaches its steady state when

$$t = \Lambda^{-\frac{1}{3}}(3x\tan\alpha)^{\frac{1}{3}}/\sin\alpha,$$

which is negligible compared to the $O(1)$ time scale of the overall settling process.

Since the essential features of the above analysis carry over to the general case, we can conclude that, within an $O(\Lambda^{-\frac{1}{3}})$ time interval, a steady interface will be reached whose shape is given by

$$\tilde{\delta}(x) = \left[\frac{3}{\cos\alpha(x)}\int_0^x \sin\alpha(x)\,dx\right]^{\frac{1}{3}} + o(1) \tag{3.11}$$

if we set $\tilde{\delta}(0) = 0$. Actually, as is common with any standard boundary-layer analysis, the above solution does not apply near the leading edge, $x = 0$, where the longitudinal and transverse scales and, therefore, the terms $\partial^2 u/\partial x^2$ and $\partial^2 u/\partial y^2$ in the x momentum equation are of comparable magnitude; consequently, although $\tilde{\delta}(0)$ must be small if the velocities in the two regions are to match, it will still be finite. In fact, its order of magnitude depends on the surface geometry near the leading edge.

Consider first the case of a surface which is locally wedge-shaped. Here α remains $O(1)$ as $x \to 0$ and hence we see from (3.11) that the thickness of the particle-free layer, $\Lambda^{-\frac{1}{3}}\tilde{\delta}$, will be $O(x)$ only if the longitudinal scale in the leading edge region is $O(\Lambda^{-\frac{1}{2}})$ and $\tilde{\delta} = O(\Lambda^{-\frac{1}{3}})$. The corresponding results for a surface for which $\alpha = O(x)$ as $x \to 0$, are that the longitudinal scale is $O(\Lambda^{-1})$ and $\tilde{\delta} = O(\Lambda^{-\frac{2}{3}})$. A somewhat more precise version of (3.11) is, therefore,

$$\tilde{\delta} = \left(\frac{C}{\cos\alpha} + \frac{3}{\cos\alpha}\int_0^x \sin\alpha\,dx\right)^{\frac{1}{3}} + o(1),$$

where C is $O(\Lambda^{-\frac{1}{2}})$ or $O(\Lambda^{-2})$ depending on the surface geometry near $x = 0$. At any rate it is evident that, for $x = O(1)$, the difference between the above and (3.11) is negligible to the degree of approximation to which the present analysis has been developed.

Up to this point, the definition of the characteristic length, l, has been kept arbitrary. However, since the process is pseudo-steady to first order (except for a short time interval initially), an appropriate choice would be H (cf. figure 2), the instantaneous

height of the suspension above the origin, because this choice assures that all stretched quantities remain $O(1)$ throughout the duration of the process. Thus, R and Λ become, respectively,

$$R \equiv \tfrac{2}{9}Ha^2 f(c_0)\rho_f(\rho_s-\rho_f)g/\mu, \quad \text{and} \quad \Lambda \equiv \tfrac{9}{2}(H/a)^2 c_0/f(c_0). \tag{3.12}$$

Of particular interest is δ_m, the maximum thickness of the particle-free layer, which in view of (3.2) and (3.11) is given approximately by

$$\delta_m = \left\{\frac{3\Lambda^{-1}}{\cos\alpha(x_m)}\int_0^{x_m}\sin\alpha\,dx\right\}^{\frac{1}{3}}, \quad \text{with} \quad \int_0^{x_m}\cos\alpha\,dx = 1.$$

Evidently, the PNK theory applies for predicting the instantaneous height of the suspension only if δ_m is much less than the length of the effectively horizontal portion of the suspension-clear fluid interface, i.e. the length BC or $B'C$ of figure 2.

3.2. *The motion within the suspension*

To complete our description of the sedimentation process, it is necessary that we examine the flow within the particle-containing region where $\phi = 1$. Here, the buoyancy term of (3.1) is absent but, in view of our analysis in § 3.1, the longitudinal velocity is $O(\Lambda^{\frac{1}{3}})$, at least close to the interface between the suspension and the particle-free layer underneath the downward-facing surface. Hence, the inertia terms are $O(R\Lambda^{\frac{2}{3}})$ which, owing to the absence of the buoyancy term, must be balanced by the viscous and, perhaps, the pressure terms of (3.1). But in most cases of practical interest, $R \geqslant O(1)$ and $\Lambda \gg 1$ [with R and Λ defined as in (3.12)] and, therefore, $R\Lambda^{\frac{1}{3}}$ the Reynolds number of the motion is large. This suggests a standard boundary-layer type analysis.

The buoyancy-induced motion in the particle-free region imparts a longitudinal velocity at the interface equal to [cf. (3.2) and (3.5a)]

$$u = \tfrac{1}{2}\Lambda^{\frac{1}{3}}\tilde{\delta}^2\cos\alpha(x), \tag{3.13}$$

where $\tilde{\delta}$ is given by (3.11). A boundary-layer type flow then develops analogous to a conventional boundary layer past a moving surface. Here, however, the characteristic Reynolds number is $\bar{R}\Lambda^{\frac{1}{3}}$ rather than $\bar{R}$ as is usually the case and hence the appropriate boundary-layer stretching transformations are

$$\bar{u} = \Lambda^{-\frac{1}{3}}u, \quad \bar{y} = (\bar{R}\Lambda^{\frac{1}{3}})^{\frac{1}{2}}y, \quad \bar{v} = \Lambda^{-\frac{1}{3}}(\bar{R}\Lambda^{\frac{1}{3}})^{\frac{1}{2}}v, \tag{3.14}$$

where $\bar{R} = R\rho(1)/\mu(1)$ is the Reynolds number based on the properties of suspension with $\phi = 1$ rather than on those of the pure fluid and x is now measured along the interface and $\bar{y}$ normal to it with $\bar{u}$ and $\bar{v}$ being the corresponding velocities. From (3.14) we see that

$$(\partial u/\partial y)_{\bar{y}=0} = (\bar{R}\Lambda)^{\frac{1}{2}}(\partial\bar{u}/\partial\bar{y})_{\bar{y}=0},$$

which will match with the corresponding term from the solution in the particle-free layer, if the second approximation to that solution, i.e. the error term in (3.5a), is set equal to $O(\bar{R}^{\frac{1}{2}}\Lambda^{-\frac{1}{6}})$. Thus, as long as $(\partial\bar{u}/\partial\bar{y})_{\bar{y}=0}$ is numerically an $O(1)$ quantity, the boundary condition (3.4c) is justified since $(\partial\tilde{u}/\partial\tilde{y})_{\tilde{y}=\tilde{\delta}}$, which was assumed to be $o(1)$, is in fact $O(\bar{R}^{\frac{1}{2}}\Lambda^{-\frac{1}{6}})$.

In terms of the scaled variables of (3.14), the momentum and continuity equations become, respectively,

$$\bar{u}\frac{\partial \bar{u}}{\partial x}+\bar{v}\frac{\partial \bar{u}}{\partial \bar{y}}=\frac{\partial^2 \bar{u}}{\partial \bar{y}^2}-\frac{1}{\bar{R}\Lambda^{\frac{2}{3}}}\frac{\partial P}{\partial x}+O(\Lambda^{-\frac{1}{3}})+O(\bar{R}\Lambda^{\frac{1}{3}})^{-1}, \tag{3.15a}$$

$$\partial P/\partial \bar{y}=O(\Lambda^{\frac{1}{3}}), \tag{3.15b}$$

and

$$\partial \bar{u}/\partial x+\partial \bar{v}/\partial \bar{y}=0. \tag{3.15c}$$

We note from (3.14) that, with $\bar{R}=O(1)$, v is $O(\Lambda^{\frac{1}{3}})$ whereas, in the particle-free layer, v is $O(1)$. Consequently, when $\Lambda \gg 1$ and with $\bar{y}=0$ denoting the interface between the two regions, we have to first order:

$$\bar{u}=\tfrac{1}{2}\delta^2\cos\alpha(x), \quad \bar{v}=0 \quad \text{at} \quad \bar{y}=0. \tag{3.16a}$$

We also require another boundary condition for $\bar{u}$ as well as an expression for $\partial P/\partial x$ which will depend, of course, on the state of motion within the bulk of the suspension and on whether the thickness of the boundary layer is much smaller than or comparable to the width of the vessel.

Let us consider first the case when the height of the suspension is much greater than the boundary-layer thickness, $(\bar{R}\Lambda^{\frac{1}{3}})^{-\frac{1}{2}}$, and also the spacing b of the plates is effectively infinite. Then since the characteristic length scale in both the x and y directions is $O(1)$ in the core of the suspension, u and v must also be of comparable order. Furthermore, the entrainment velocity into the boundary layer must be of the same order as the boundary-layer velocity v so both u and v must be $O(\bar{R}^{-\frac{1}{2}}\Lambda^{\frac{1}{3}})$ within the bulk of the suspension. Consequently, the second boundary condition for $\bar{u}$ is

$$\bar{u}=0 \quad \text{at} \quad \bar{y}=\infty. \tag{3.16b}$$

Also, from (3.1) we see that the flow within the core is inviscid with a pressure of $O(\Lambda^{\frac{1}{3}})$; hence, on account of (3.15*b*) the pressure is $O(\Lambda^{\frac{1}{3}})$ everywhere within the boundary layer and, therefore, can be neglected in (3.15*a*).

Even with this last simplification, however, the system (3.15)–(3.16) can, in general, be solved only numerically; but, in the special case of constant α (which corresponds to the commonly used geometry of an inclined planar surface) a similarity solution applies. Specifically, on account of (3.11) and (3.16*a*) we let

$$\bar{u}=\tfrac{1}{2}(3x\tan\alpha)^{\frac{2}{3}}(\cos\alpha)f'(\eta), \quad \eta\equiv \bar{y}/g(x), \tag{3.17}$$

which, when substituted into (3.15)–(3.16), yields

$$g(x)=[\tfrac{5}{12}(3\tan\alpha)^{\frac{2}{3}}\cos\alpha]^{-\frac{1}{2}}x^{\frac{1}{2}},$$

$$\bar{v}=\left(\frac{9^{\frac{1}{3}}}{60}\cos\alpha\right)^{\frac{1}{2}}(\tan\alpha)^{\frac{1}{3}}x^{-\frac{1}{6}}(\eta f'-5f)$$

and

$$f'''+ff''-\tfrac{4}{5}(f')^2=0, \tag{3.18}$$

with boundary conditions $f(0)=0$, $f'(0)=1$, and $f'(\infty)=0$. Equation (3.18) will be recognized as the familiar Falkner–Skan equation without the term arising from the pressure; also, the boundary conditions are different. This boundary value problem was solved numerically and the resulting functions $f'(\eta)$ (which is proportional to $\bar{u}$) and $(5f-\eta f')/6$ (which is proportional to $-\bar{v}$) are shown in figure 3. We note that f'

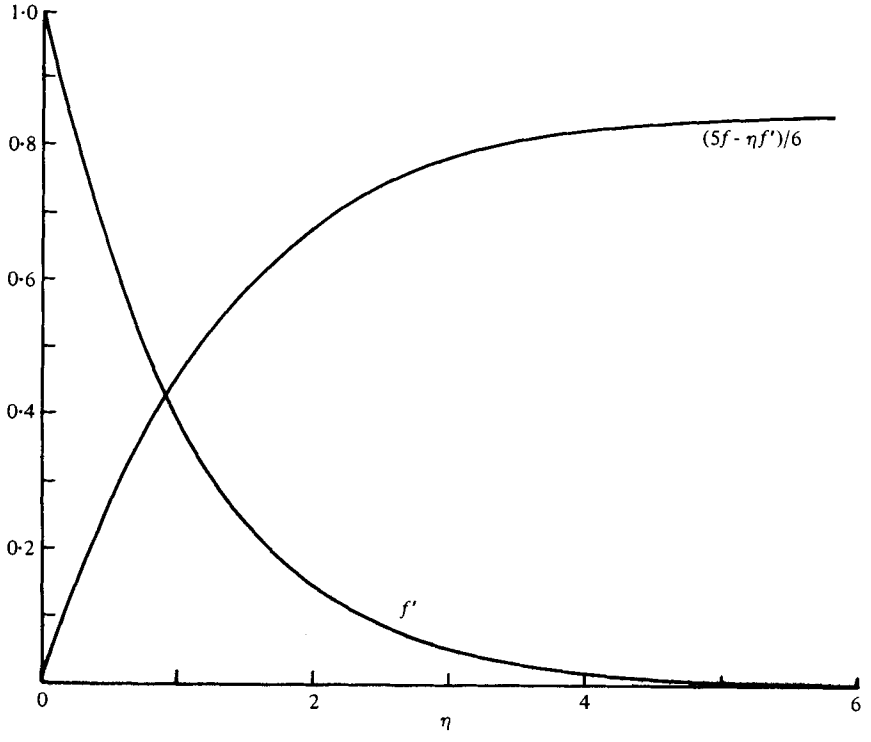

FIGURE 3. The solution of equation (3.14) where $f'(\eta) \propto \bar{u}$ and $(5f - \eta f')/6 \propto -\bar{v}$.

decreases monotonically from 1 to 0 with f approaching asymptotically the expression $1{\cdot}023 - 1{\cdot}07e^{-1{\cdot}023\eta}$ as $\eta \to \infty$.

If, on the other hand, the spacing of the plates is decreased, the large velocity at the clear-fluid interface may set the bulk of the suspension into a rapid circulating motion similar to that observed in closed cavities with one moving wall (cf. Pan & Acrivos, 1966). In fact, for very large values of $\bar{R}\Lambda^{\frac{1}{3}}$, the effective Reynolds number for the flow in the suspension, the motion should resemble the well-known Batchelor (1956) model of high Reynolds number steady flow with closed streamlines; i.e. a constant vorticity inviscid core surrounded by a thin boundary layer.

Indeed, a mathematical description of the flow along the lines of Batchelor's model can be constructed without too much effort. The velocities in the bulk of the suspension will now be $O(\Lambda^{\frac{1}{3}})$, and the flow will be inviscid; also the pressure will be $O(\bar{R}\Lambda^{\frac{2}{3}})$ and hence, in general, must be retained in (3.15a). Let us consider the case of the parallel plate geometry and let us suppose for the sake of simplicity that the aspect ratio of the core region, i.e. the ratio of its length to its breadth, is large. Under these conditions the streamlines of the inviscid constant vorticity flow in the core are effectively parallel to the inclined walls of the container, the pressure is constant, and the corresponding longitudinal velocity is given by

$$u = \omega b(\tfrac{1}{2} - yH/b), \tag{3.19}$$

where ω is the unknown dimensionless uniform vorticity in the core. This core is separated from the interface between the particle-free region underneath the down-

ward-facing step and the suspension by the boundary layer studied earlier within which the velocity still satisfies (3.15) and (3.16*a*) plus

$$\bar{u} \to \tfrac{1}{2}\Lambda^{-\frac{1}{3}}\omega b \quad \text{as} \quad \bar{y} \to \infty,$$

in lieu of (3.16*b*). It is evident that a similarity solution to the boundary-layer equations no longer applies.

Now, as shown by Batchelor (1956, p. 184), the value of the uniform vorticity ω can be determined with ease when the pressure along the boundary layer surrounding the inviscid core is constant, which, in view of (3.19), is also the case here. Hence, on using Batchelor's equation (3.6), assuming that, within the boundary layer, $\bar{u} = 0$ at the surface of the upward-facing wall† and neglecting any end effects in the dual limit $b/H \ll 1$, $(\bar{R}\Lambda^{\frac{1}{3}})^{-\frac{1}{2}} \ll b/H$,

$$\frac{\omega b}{2} = \left(\frac{1}{2}\int_0^{\cos^{-1}\alpha} U^2\, dx\right)^{\frac{1}{2}}, \tag{3.19a}$$

where, in view of (3.13), $U = \frac{1}{2}\Lambda^{\frac{1}{3}}\tilde{\delta}^2\cos\alpha$, with $\tilde{\delta}$ given by (3.11). On evaluating these various expressions for constant α, we thus arrive at

$$\frac{\omega b}{2} = \Lambda^{\frac{1}{3}}\left[\frac{3^{\frac{7}{3}}}{56}\cos^{-\frac{5}{3}}\alpha\sin^{\frac{4}{3}}\alpha\right]^{\frac{1}{2}}.$$

So far we have only considered cases where the spacing of the plates is much larger than the thickness of the boundary layer, i.e. $b/H \gg (\bar{R}\Lambda^{\frac{1}{3}})^{-\frac{1}{2}}$. When this condition no longer holds (as was the case in our experiments to be described in § 4), equations (3.15) apply everywhere within the suspension (except of course within singular regions near the top and bottom) but the boundary condition at $\bar{y} \to \infty$ must be replaced with

$$\bar{v} = 0, \quad \bar{u} = -\bar{U}_s(x) \quad \text{at} \quad \bar{y} = (\bar{R}\Lambda^{\frac{1}{3}})^{\frac{1}{2}}b(x)/H,$$

where $y = b(x)/H$ is the dimensionless equation for the position of the upward-facing surface and $\bar{U}_s(x)$ must be determined by examining the motion of the concentrated sediment layer on the upward-facing surface. In this case the pressure will be $O(\bar{R}\Lambda^{\frac{2}{3}})$ and must be obtained from (3.15) as part of the solution.

We have shown then that for all of these possible flow regimes the pressure in the bulk of the suspension is at most $O(\bar{R}\Lambda^{\frac{2}{3}})$ while the change in the pressure across the boundary layer is only $O(\Lambda^{\frac{1}{3}})$. Thus, the pressure at the interface between the clear fluid layer and the suspension can be at most $O(\bar{R}\Lambda^{\frac{2}{3}})$ which, together with (3.3*b*), justifies our earlier step of neglecting the pressure term in (3.3*a*) when solving for the flow within the clear-fluid layer. These results can also be used to deduce some useful information concerning the shape of the interface at the top of the suspension (i.e. the segment $B'C$ in figure 2). For, as is evident from (3.1*a*), the presence of the particles increases the dimensionless pressure gradient by an $O(\Lambda)$ amount, and, therefore, the change in the vertical height across the top of the suspension will be at most $O(\Lambda^{-\frac{2}{3}})$ if the spacing of the plates is very large, and $O(\bar{R}\Lambda^{-\frac{1}{3}})$ otherwise. Thus, as $\Lambda \to \infty$ and $\bar{R}$ remains fixed, the top of the suspension becomes horizontal.

Up to this point, we have confined our discussion to the case in which $\bar{R}\Lambda^{-\frac{1}{3}} = o(1)$.

† Actually this condition should be replaced by the requirement that $u = -U_s(x)$, the velocity of the sediment layer. Since the latter may be large, (3.19*a*) may underestimate the value of ω.

Under some conditions, however, the Reynolds number $\bar{R}$ may be moderately large so that the parameter $\bar{R}\Lambda^{-\frac{1}{3}}$ could be, numerically, an $O(1)$ quantity. This results in the following modifications of our analysis:

The basic equations and stretching transformations derived in this section remain unchanged except that the right-hand side of (3.3*a*) must now be retained. In addition, $\tilde{\delta}$, the thickness of the particle-free region, as well as the associated velocities $\tilde{u}$ and $\tilde{v}$ are no longer independent of the flow within the suspension for, besides (3.4*a*) and (3.4*b*), the boundary conditions at the interface are the following.

(*a*) Continuity of velocity:

$$\left.\begin{aligned} \tilde{u}(\text{at } \tilde{y} = \tilde{\delta}) &= \bar{u}(\text{at } \bar{y} = 0), \\ \tilde{v}(\text{at } \tilde{y} = \tilde{\delta}) &= (\bar{R}\Lambda^{-\frac{1}{3}})^{-\frac{1}{2}}\,\bar{v}(\text{at } \bar{y} = 0). \end{aligned}\right\} \tag{3.20a}$$

(*b*) Continuity of shear stress:

$$(\partial\tilde{u}/\partial\tilde{y})_{\tilde{y}=\tilde{\delta}} = \mu(1)\,(\bar{R}\Lambda^{-\frac{1}{3}})^{\frac{1}{2}}\,(\partial\bar{u}/\partial\bar{y})_{\bar{y}=0}. \tag{3.20b}$$

Thus, clearly, $\tilde{\delta}$, $\tilde{u}$, $\tilde{v}$, $\bar{u}$, and $\bar{v}$ must be obtained simultaneously. Unfortunately, the similarity solution no longer exists even if α, the local angle of inclination, is a constant, but, of course, the appropriate system of equations plus boundary conditions can easily be solved numerically using standard routines.

We note that when $b/H \gg 1$ the flow within the bulk of the suspension will now be viscous, since the corresponding velocities will be $O(\bar{R}\Lambda^{-\frac{1}{3}})^{-\frac{1}{2}}$, i.e. $O(1)$, rather than $O(\Lambda^{\frac{1}{3}})$ as was the case before when $\bar{R}$ was $O(1)$. The reason for this decrease is that, when $\bar{R}$ is large, the thickness of the boundary layer will be $O(\bar{R}^{-\frac{1}{2}})$ smaller, and, hence, the rate of fluid entrainment will also be correspondingly smaller. On the other hand, when the bulk of the suspension is circulating rapidly or when the boundary layer extends all of the way across the container, the pressure in the suspension, $O(\bar{R}\Lambda^{\frac{2}{3}})$, will now be $O(\Lambda)$. Therefore, the pressure term must be retained in (3.3*a*) and hence the equations describing the flow in each of the two regions must be solved simultaneously.

A final possible flow regime can exist when the spacing of the plates is of the same order as the thickness of the clear-fluid layer, i.e. when $b/H \sim O(\Lambda^{-\frac{1}{3}})$. Then the stress within the suspension is comparable to that in the clear-fluid layer so the boundary condition (3.4*c*) must be suitably modified. Also, the pressure becomes $O(\Lambda)$ and must be determined as part of the solution. Thus, once again, the equations describing the flow in each of the two regions must be solved simultaneously; however, the analysis simplifies because, to first-order, the flow is essentially parallel. In fact, a number of interesting phenomena can occur and since, as seen from (1.2), the greatest augmentation to the settling rate is obtained in long narrow tubes (i.e. when $b/H \ll 1$), this case will be considered separately in another publication.

We close this section by examining briefly the flow in the concentrated sediment layer on the upward-facing surface. As mentioned in § 2, the fact that ϕ must attain its maximum value at this surface results in the creation of concentration gradients which could propagate back into the bulk of the suspension along the particle streamlines. However, in regions where $\phi > 1$, the large buoyancy term in (3.1) tends to induce a downward motion. In fact, the flow here is analogous to that in the clear-fluid layer in that the buoyancy term can be balanced only in a thin viscous layer immediately adjacent to the upward-facing surface. But, whereas in the latter the inter-

face is self-sharpening so that the concentration distribution is known, in the sediment layer the concentration varies continuously and must be determined as part of the solution.

Although a detailed solution for this problem has not been worked out, the same type of scaling arguments as used above show that the longitudinal velocity is, in order of magnitude, inversely proportional to the thickness of the sediment layer which must scale as $[\Lambda(\phi_1 - 1)/\mu(\phi_1)]^{-\frac{1}{3}}$ where $\phi_1 > 1$ is an appropriate average value of ϕ in the layer. Thus, when $\Lambda \gg 1$ and provided that $\mu(\phi_1)$ does not become too large, the layer immediately adjacent to the upward-facing surface is very thin. We note that although the velocity at the edge of the sediment layer is $O(\Lambda^{\frac{1}{3}})$, the large value of ϕ_1, which implies a very large viscosity $\mu(\phi_1)$, may render the numerical value of this sediment velocity appreciably smaller than the maximum velocity within the clear-fluid layer.

4. Experimental observations

Several batch inclined settling experiments were conducted in our laboratory using a parallel-plate geometry as pictured in figure 1. The suspending medium consisted of a mixture of Union Carbide UCON oils and Monsanto HB40 hydrogenated terphenyl oil which gave a Newtonian fluid with density 0·992 g/ml and viscosity 0·677 P at 21·6 °C, the nominal temperature of the experiments. The particles were close-sized spherical glass beads with mean diameter 137 μm and density 2·42 g/ml. The experiments were conducted by adding the desired amount of suspension to the vessel, mixing the suspension for several minutes in order to render the initial concentration distribution more or less uniform, and then removing the mixer and allowing the particles to settle. A relatively sharp interface between the suspension and the particle-free fluid formed almost immediately and the vertical height of the suspension, H, as well as the height of the concentrated sediment layer at the bottom of the vessel were measured as functions of time using a cathetometer. The spacing of the plates, b, was 5 cm but the other parameters were varied systematically to cover the following range of conditions:

$$2 \leqslant H_0/b \leqslant 8; \quad 0° \leqslant \alpha \leqslant 50°; \quad 0{\cdot}76 \leqslant R_0 \leqslant 3{\cdot}04;$$
$$4{\cdot}8 \times 10^5 \leqslant \Lambda_0 \leqslant 1{\cdot}5 \times 10^7; \quad 0{\cdot}01 \leqslant c_0 \leqslant 0{\cdot}10.$$

Under these conditions both the translational and shear particle Reynolds number was at most $O(10^{-3})$ throughout the flow field. Also, although the aspect ratio b/H was much larger than $\Lambda^{-\frac{1}{3}}$, it was only two to three times larger than $(R\Lambda^{\frac{1}{3}})^{-\frac{1}{2}}$ thereby implying that the boundary layer in the suspension extended across most of the vessel. Thus the analysis of § 3, and specifically (3.5a), (3.5b) and (3.11), would be expected to accurately describe the flow in the clear-fluid layer and its thickness; on the other hand, since (3.16b) would not be applicable in this case, the observed flow pattern could differ quantitatively from that given by the solution of (3.18).

Some typical experimental results for the height of the suspension as a function of time are plotted in figure 4 together with the corresponding predictions of the PNK theory for c_0 equal to 0·10 and with $H_0/b = 8$. The dashed lines in these figures are the integrated forms of (1.2) and the experimental data are seen to deviate somewhat from the theory. This discrepancy is due to the fact that the above theoretical

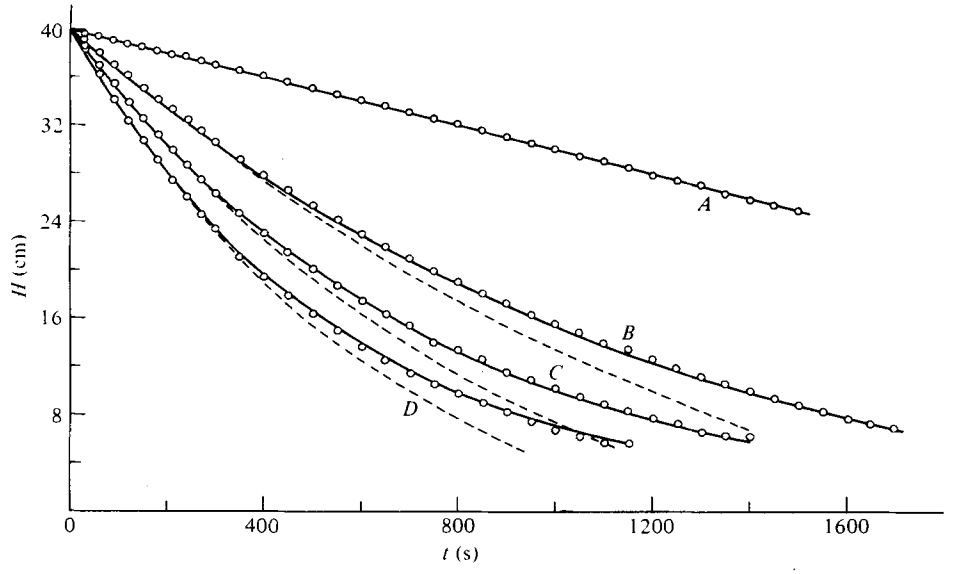

FIGURE 4. Height of the top interface H versus time for $c_0 = 0{\cdot}10$, $H_0 = 40$ cm, and $b = 5$ cm ($\Lambda_0 = 3{\cdot}27 \times 10^7$, $R_0 = 0{\cdot}560$) for different angles of inclination α: A, $\alpha = 0°$; B, $\alpha = 20°$; C, $\alpha = 35°$; D, $\alpha = 50°$. - - -, ordinary PNK theory; ——, PNK predictions accounting for the sediment layer.

predictions do not account for the existence of the concentrated sediment region at the bottom of the vessel. Specifically, in deriving (1.2), the interface between the clear fluid and suspension was assumed to intersect the walls of the container at the origin which was taken as the point of intersection between the downward and upward-facing surfaces (cf. figure 2). This assumption is correct as long as the level of the concentrated sediment layer does not rise above this point. When this is no longer the case, however, the variable H on the right-hand side of (1.2) should be replaced by $H - H_s$, where H_s refers to the height above the origin of the intersection between the top of the sediment layer and the downward-facing surface. By assuming a value for the volume fraction in the sediment c_s and applying arguments analogous to those in § 1 to the sediment region, the PNK theory can easily be extended to include this effect. The results are shown as the solid lines in figure 4 and the agreement between theory and experiment is clearly excellent.

The value of c_s was calculated directly from the experimentally measured heights H and H_s (both interfaces were essentially horizontal throughout the settling process) using a simple mass balance on the particles. The clear-fluid layer and thin sediment layer on the upward-facing surface were neglected and the concentrations in the suspension and sediment were both assumed to be uniform with values of c_0 and c_s, respectively. Unfortunately, c_s was found to increase with time during a given experiment (a typical range was $c_s = 0{\cdot}43$ to $0{\cdot}53$) and, between experiments, to increase with the angle of inclination α and the initial concentration (the range of the average values was $c_s = 0{\cdot}46$ to $0{\cdot}55$). The variation in c_s with time in a given experiment is probably due to the fact that the average concentration in the sediment layer on the upward-facing surface is relatively low (say $c \approx 0{\cdot}40$). Then, after it flows off the wall, this sediment can slowly compact while remaining at the bottom of the vessel. This

conjecture is consistent with the experimental observations that the sediment on the wall flowed freely – indicating that the concentration there was not too large – and that after the settling process was complete, the sediment in the bottom of the container continued to compact. It is also likely that the concentration in the thin layer on the wall depends somewhat on the conditions of the experiment, thereby explaining the variation in c_s between experiments.

In calculating the theoretical curves in figure 4, the average value of c_s for each experiment was used. It should be clearly kept in mind, however, that c_s was determined directly from the experimental data and not from a comparison of the theory and experiments. The only other quantity needed for the theoretical calculations was v_0, the settling velocity of the particles, which was obtained from independent vertical settling measurements using the same suspension as in the inclined settling experiments. These values for v_0 were found to lie, typically, within 5% of those derived from Barnea & Mizrahi's (1973) correlation for the vertical settling rate as a function of concentration. Thus, it should be emphasized that the theoretical curves were obtained without the use of any adjustable parameters.

In addition, our qualitative observations of the flow field can be summarized as follows. First of all, it appeared that the boundary of the particle-free layer under the downward-facing surface formed immediately after the mixing had ceased and that the flow within this region reached a steady state after only a few seconds. Moreover, at the start of the process when the region of particle-free fluid above the suspension was very thin, the interface between clear fluid and suspension remained very close to the surface of the downward-facing step all the way to the top of the suspension, where, after making a sharp turn, it became horizontal. At later times however, this layer began to broaden gradually at a distance of about 2 cm below the horizontal part of the interface, no doubt because the fluid had to slow down as it approached the region of pure liquid above the suspension. Of course, when this region is shallow, continuity requires that the longitudinal velocity be large, but when its depth becomes $O(1)$, then both velocity components should be of the same order, i.e. $O(1)$, and, again owing to continuity, the particle-free fluid slit ought to broaden under these conditions. At any rate, as was said earlier, this broadening effect was confined to a distance of about 2 cm from the top of the suspension, and hence the analysis of § 3 should apply over most of the length of the clear-fluid layer.

The measured thickness of this layer as a function of the distance along the downward-facing surface is shown in figure 5 along with the theoretical result (3.11) for $c_0 = 0{\cdot}05$ and $0{\cdot}10$ and with $\alpha = 45°$. Clearly, the agreement is very good. As seen in § 3.1, the theory predicts that, after a short initial period, the thickness of this layer at a given point on the downward-facing surface should be independent of both time and the instantaneous height of the suspension. This was indeed found to be the case everywhere except near the top of the suspension, where the width of the slit at a given point increased with time as the top of the suspension approached. (The broadening of the slit is not evident in figure 5 because all of the data shown there were taken when the point of observation was well below the top of the suspension.) Furthermore, the data were obtained from several different experimental runs thereby showing the reproducibility of the results.

Measurements of the velocity field are considerably more difficult to perform and, at this point, we can only offer some qualitative information which was obtained by

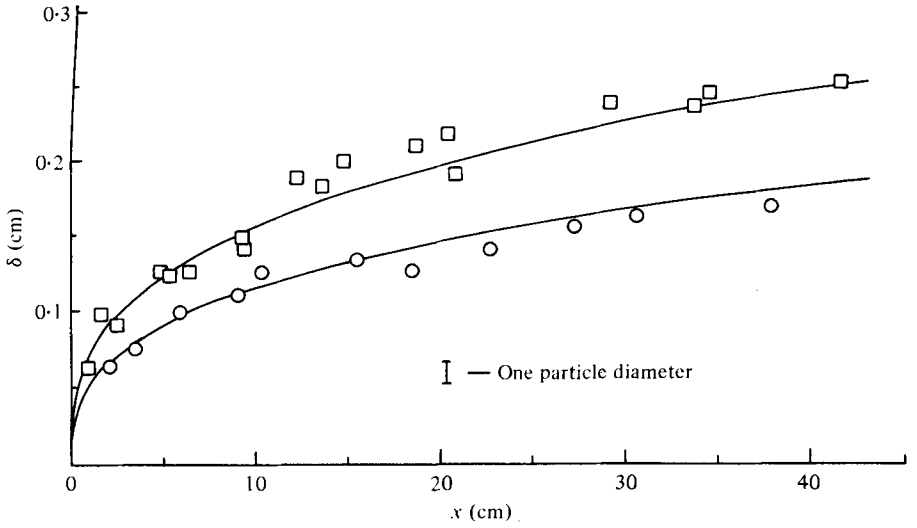

FIGURE 5. The width of the clear-fluid layer versus the distance along the downward-facing surface for a parallel plate geometry with $\alpha = 45°$. □, $c_0 = 0{\cdot}05$; ○, $c_0 = 0{\cdot}10$. The lines show the corresponding theoretical predictions.

visually observing the motion of the particles. First of all, the largest velocities were found near the interface between the clear-fluid layer underneath the downward-facing surface and the suspension. This velocity was directed along the interface and its magnitude increased from essentially zero at the bottom of the vessel to a maximum value near the top of the suspension which was visually estimated to be one or two orders of magnitude larger than the vertical settling velocity. Furthermore, comparison of the velocities of the few particles which were trapped in the clear-fluid layer with those of the particles on the interface indicated that, at any given x, the maximum velocity in the slit occurred very close to the interface as predicted by (3.4c).

The flow field in the particle-containing region was considerably more complex and several interesting phenomena were observed. At the start of some of the experiments, a rapid circulating motion developed throughout most of the suspension. This flow did not conform to the model of an inviscid core with constant vorticity studied in § 3, because in these experiments $b/H \approx (R\Lambda^{\frac{1}{2}})^{-\frac{1}{2}}$ and the boundary layer extended all of the way across the vessel. Therefore, in the present case, the observed circulation was undoubtedly due to continuity which requires that there be no net flow across a plane of constant x; hence the upward flow of the suspension caused by the motion of the clear-fluid layer must be accompanied by a corresponding downward flow elsewhere in the suspension.

At any rate, this rapid motion within the core persisted for only a short time, apparently ceasing when the clear fluid above the suspension was no longer shallow. In fact, the circulating flow gave way to one in which the particle motion was relatively slow everywhere except in a thin layer adjacent to the clear-fluid slit beneath the downward-facing surface. The thickness of this region was difficult to determine but appeared to be approximately five times that of the clear-fluid layer. The particles close to the clear-fluid slit were observed to rise rapidly, come to an abrupt stop at the top of the suspension, and then descend rapidly in a thin layer immediately adjacent

to that where the particles were rising. Meanwhile, the primary flow in the core was much slower with the particles moving primarily down the vessel. Also, near the top of the suspension, thin streams of rapidly moving suspension were observed to break away from the main flow and to descend rapidly into the bulk of the suspension. As these streams travelled into the suspension they dominated the flow locally, but as they seemed to die out rapidly they did not affect the motion further down in the vessel. Unfortunately, we have been unable, to date, to arrive at a satisfactory explanation for this behaviour.

5. Discussion

Besides leading to quantitative results, the analysis of § 2 and 3 also provides a clear and fairly complete understanding of how the inclined settling process operates. Initially the vessel is completely filled with suspension and the presence of the particles creates an $O(\Lambda)$ dimensionless hydrostatic pressure gradient in the vertical direction. But, since the particles are more dense than the fluid, they tend to settle vertically thereby creating a layer of particle-free fluid underneath the downward-facing surface. Evidently, this fluid does not experience the extra $O(\Lambda)$ body force due to the particles and hence, owing to buoyancy, flows upward along the wall; moreover, on account of continuity, it is replaced by new fluid which is entrained from the suspension into the particle-free layer. This fluid motion towards the downward-facing surface creates a drag on the particles which balances the component of the gravitational force tending to make them move away from the wall. In turn, this leads to a clear-fluid layer which remains thin and independent of time when $\Lambda \gg 1$.

We also note that since the interface between the suspension and the particle-free fluid is everywhere upward-facing and since when the particle Reynolds number is small the particle velocity equals the fluid velocity plus a slip velocity in the direction of gravity, once fluid leaves the particle-containing region it cannot re-enter it. This must be the case because in any region where the fluid velocity at the interface includes a component directed into the suspension, the particles on the interface move with this velocity plus a slip velocity which is also directed into the suspension. Hence, since the position of the interface is determined by the presence of particles, the interface moves so as to prevent the entry of the fluid into the suspension. Thus, the entrainment of fluid into the clear-fluid layer results in an enhancement of the rate at which particle-free fluid is produced over that in a vertical vessel with the same spacing between the plates.

An analogous process occurs at the upward-facing surface where the settling particles accumulate to form a concentrated sediment layer. Here, the concentrated sediment is denser than the suspension in the core and hence flows down the wall to the bottom of the vessel where it can be collected and removed. This results in a sediment layer which remains thin when $\Lambda \gg 1$. Finally, the rising fluid in the clear-fluid layer and the falling sediment layer drive a flow within the suspension whose structure is determined by the relative magnitude of $\bar{R}$, Λ, and b/H. As we saw from the analysis of § 2, however, the enhancement to the settling rate does not result from this convective motion but is rather due to the increase in the surface area that is available for creating particle-free fluid (or, conversely, for collecting particles).

Nevertheless, the convective motion within the tank does have important

consequences as regards the feasibility of using the Boycott effect for designing efficient continuous settlers. The use of inclined settling for continuous systems is possible only if steady solutions to the flow field equations can be shown to exist; in particular, the position of the interface between the clear fluid and suspension must be stationary. Such solutions do not exist for all sets of conditions however. For instance, consider the limiting case $\Lambda \to 0$. Then, for the batch process, a solution of (3.1) satisfying the condition of no slip at the walls is $\mathbf{u} \equiv 0$; i.e. there would be no bulk motion and the particles would merely settle vertically. Thus, the only way to produce a continuous settler out of the system would be to operate it as a slanted vertical settler; that is to add new suspension and remove clear fluid and sediment uniformly at every point along the vessel. Obviously, this is not practical.

On the other hand, we found in § 3 that, when Λ is large and $R = O(1)$, the interface along the downward-facing wall is stationary while that at the top of the vessel is essentially horizontal. Also, the concentrated sediment forming on the upward-facing surface flows down the wall so that the thickness of this layer remains thin throughout the process (provided, of course, that the viscosity of the sediment does not become too large). It should be possible in this case therefore, to achieve a steady flow pattern by just adding enough new suspension to the core to replace that which is settling out while removing clear fluid and sediment from the top and bottom of the vessel, respectively. Furthermore, since the flow in the suspension is relatively fast, the details of how the feed is added would be unimportant to a first approximation. Thus, continuous operation in an inclined settling vessel seems feasible provided that Λ is large and the flow remains laminar.

We close by considering the important question regarding the range of applicability of the PNK theory for designing settling vessels. In § 2 we showed that, in the limit of negligibly small particle Reynolds numbers, the PNK theory predicts the correct volumetric settling rate for monodisperse suspensions provided only that the particle-containing region covers the entire upward-facing surface below the top of the suspension. This condition is satisfied if the width of the clear-fluid layer is small at $x = 0$, i.e. that X_0 is negligible compared to X_1 in (2.10). As was shown in § 3, this is the case if $\Lambda^{-\frac{1}{2}} \ll 1$. Furthermore, the analysis of § 3 also shows that, as $\Lambda \to \infty$, the thickness of the clear-fluid slit vanishes, the top of the suspension becomes flat and that, consequently, the PNK prediction for the velocity of the interface at the top of the suspension applies in this limit. We also note that these results are independent of the details of the flow field provided, of course, that the flow remains laminar and that a stable interface exists between the particle-free regions and the suspension.

In most industrial applications, the height of the settling vessel is typically on the order of a few metres while, owing to the small size of the particles being settled, the particle settling velocity and Reynolds number are low. Under these conditions, Λ is typically 10^6 or larger while R remains of order 1–10^2; therefore, the PNK theory should be adequate for the design of both continuous and batch settling tanks for clarifying suspensions.

It appears then that the primary factor which would cause significant deviations from the PNK theory is an instability of the interface between the suspension and the particle-free layer which would cause entrainment of particles into the rapidly rising fluid stream. If such remixing were to occur, the fluid above the suspension would become contaminated with particles and its quality would be correspondingly reduced.

Hence, if the criterion for operating a continuous settler requires a pure fluid overflow, a large reservoir above the suspension would have to be maintained, to allow these resuspended particles to resettle, and the operating efficiency of the settling vessel would diminish appreciably. The expressions derived in this paper for the flow field in the vicinity of this interface are therefore of value because they could serve, in principle, as the starting point for a stability analysis that would delineate the conditions under which inclined settling devices could be operated continuously.

This work was supported in part by contract EPRI RP 314-1 with the Electric Power Research Institute in Palo Alto, California.

REFERENCES

BARNEA, E. & MIZRAHI, J. 1973 A generalized approach to the fluid dynamics of particulate systems. Part 1. General correlation for fluidization and sedimentation in solid multiparticle systems. *Chem. Engng J.* **5**, 171–189.

BATCHELOR, G. K. 1956 On steady laminar flow with closed streamlines at large Reynolds number. *J. Fluid Mech.* **1**, 177–190.

BOYCOTT, A. E. 1920 Sedimentation of blood corpuscles. *Nature*, **104**, 532.

GRAHAM, W. & LAMA, R. 1963 Sedimentation in inclined vessels. *Can. J. Chem. Eng.* **41**, 31–32.

HILL, W. D. 1974 Boundary-enhanced sedimentation due to settling convection. Ph.D. thesis, Carnegie–Mellon University, Pittsburgh, Pa.

HILL, W. D., ROTHFUS, R. R. & LI, K. 1977 Boundary-enhanced sedimentation due to settling convection. *Int. J. Multiphase Flow* **3**, 561–583.

KINOSITA, K. 1949 Sedimentation in tilted vessels. *J. Colloid Interface Sci.* **4**, 525–536.

KYNCH, G. J. 1952 A theory of sedimentation. *Trans. Faraday Soc.* **48**, 166–176.

NAKAMURA, H. & KURODA, K. 1937 La cause de l'accélération de la vitesse de sédimentation des suspensions dans les récipients inclinés. *Keijo J. Med.* **8**, 256–296.

OLIVER, D. R. & JENSON, V. G. 1964 The inclined settling of dispersed suspensions of spherical particles in square-section tubes. *Can. J. Chem. Engng* **42**, 191–195.

PAN, F. & ACRIVOS, A. 1967 Steady flows in rectangular cavities. *J. Fluid Mech.* **28**, 643–655.

PEARCE, K. W. 1962 Settling in the presence of downward facing surfaces. *Proc. 3rd Congr. Eur. Fed. Chem. Engng, Lond.* pp. 30–39.

PONDER, E. 1925 On sedimentation and rouleaux formation. *Quart J. Expt. Physiol.* **15**, 235–252.

VOHRA, D. K. & GHOSH, B. 1971 Studies of sedimentation in inclined tubes. *Ind. Chem. Engng* **13**, 32–40.

ZAHAVI, E. & RUBIN, E. 1975 Settling of solid suspensions under and between inclined surfaces. *Ind. and Engng Chem., Proc. Design and Dev.* **14**, 34–41.